Solar Energy Vol. 50, No. 2, pp. 155–166, 1993
Printed in the U.S.A.

0038-092X/93 $6.00 + .00

PERFORMANCE STUDY OF ONE-DIMENSIONAL MODELS FOR STRATIFIED THERMAL STORAGE TANKS

E. M. KLEINBACH, W. A. BECKMAN, and S. A. KLEIN
Solar Energy Laboratory, 1500 Johnson Drive, University of Wisconsin–Madison, Madison, WI 53706, U.S.A.

Abstract—Two basic approaches are used to model the temperature distribution in thermal storage tanks for solar domestic hot water (SDHW) systems. In the multinode approach, the tank is divided into N nodes, with an energy balance written for each node. This approach results in a set of N differential equations that can be solved for the temperatures of the nodes as a function of time. In the plug flow approach, segments of liquid of different temperatures and sizes are assumed to move through the tank in a plug flow manner. The sizes of the fluid elements are determined mainly by the simulation time step and the flow rates. Whenever the incoming fluid from the heat source is colder than the fluid at the top of the tank, "plume entrainment" occurs. A model describing plume entrainment has been incorporated into both the multinode and the plug flow models in the TRNSYS program[1]. A performance study of the TRNSYS tank models has been carried out with experimental data from two different sources. Three performance numbers have been defined for quantifying the accuracy of the models compared with experimental data. Recommendations are given as to which tank model should be used under which conditions.

1. INTRODUCTION

Stratification in a thermal storage tank depends mainly on the volume of the tank; the size, location, and design of the inlets and outlets; and the flow rates of entering and leaving streams. There are four primary "destratification factors," which contribute to the loss and/or degradation of the stored energy: (a) heat losses to ambient; (b) heat conduction from the hot layer to the cold layer; (c) vertical conduction in the tank wall which along with (a) induces convective currents (mixing); and (d) mixing introduced during charge and discharge cycles. Factor (d) is generally the major cause of destratification.

The thermal performance of a solar domestic hot water (SDHW) system depends on the temperature distribution in the storage tank, which (for a specific tank) is affected mainly by the collector flow rate. High collector flow rates (>50 kg/h − m^2 collector area) have been traditionally used in forced-flow SDHW systems. High collector flow rates increase the collector heat removal factor, as explained in Duffie and Beckman[2]. However, high collector flow rates can result in short tank-turnover times, which cause mixing, resulting in a nearly uniform temperature in the storage tank. Reducing the collector flow rate lowers the collector heat removal factor but also tends to increase tank thermal stratification, which may improve the overall system performance[3,4].

To relate high and low collector flow rates with the tank size, a mean number of tank turnovers, which gives an indication of the amount of mixing caused by the collector flow, T, has been defined as

$$T = \frac{M_{heat} + M_{load}}{M_T}. \quad (1)$$

M_{heat} represents the total daily mass of the fluid coming from the heat source, and M_{load} stands for the total daily mass of the fluid removed to the load. M_T represents the mass of the fluid in the tank. Using this measure, low flow systems are defined by values of T up to about five, and high flow systems have values of T greater than five.

A number of models of differing complexity have been developed to account for thermal stratification in hot liquid storage tanks[1,5–9]. Validation of tank models has been done by comparing the thermocline (region of steepest temperature gradient inside the tank) predictions with the experimentally measured thermocline during single charge or discharge experiments. The justification of this method is that if a model is capable of accurately predicting the thermocline during charging or discharging, then it will also predict the correct temperature of the fluid being displaced (and therefore the temperature of the fluid leaving the tank) as a function of time. In this paper, a different approach of validating the storage tank models is used that does not use the thermocline.

2. STRATIFIED STORAGE TANK MODELS

2.1 *Multinode model*

In the multinode approach[1,2,6], the tank is modeled as N fully mixed volume segments (nodes). The degree of stratification is determined by the choice of N. Higher values of N result in more stratification. A maximum number of 15 nodes can be chosen in the current TRNSYS implementation. For the special case of $N = 1$, the tank is modeled as a fully mixed tank and no stratification effects are possible. Unequal size nodes can be specified. The model also provides the option of specifying fixed or variable inlet positions. For fixed inlet positions, the fluid from the heat source enters just below the auxiliary, if present, or at the top of the tank. The mains water enters at the bottom of the tank. At the end of the time step, any temperature

inversions that result from these flows are eliminated by mixing appropriate nodes. For variable inlet positions, the flows enter the nodes that are closest in density, i.e., temperature and no temperature inversions are created. This mode of operation preserves the maximum possible degree of stratification for the selected number of nodes.

An assumption employed in the multinode model is that the fluid streams flowing up and down from each node are mixed before they enter each node. In terms of Fig. 1, this assumption implies that $\dot{m}_1$ is added to $\dot{m}_4$; $\dot{m}_2$ is added to $\dot{m}_3$; and a resultant flow, either up or down, is determined before an energy balance on the nodes is done. With this assumption, the heat source and the load flow are treated simultaneously.

An energy balance written about the i-th tank node is

$$M_i C_f \frac{dT_i}{dt} = \alpha_i \dot{m}_{heat} C_f (T_{heat} - T_i) + \beta_i \dot{m}_{load} C_f (T_{mains} - T_i) + \delta_i \gamma_i C_f (T_{i-1} - T_i) + (1 - \delta_i)\gamma_i C_f (T_i - T_{i+1}) + \epsilon \dot{Q}_{aux,i} - (1 - \epsilon) UA_{fl,i} (T_i - T_{fl}) - UA_i (T_i - T_{env}) \quad (2)$$

where

$\alpha_i = 1$, if fluid from heat source enters node i, 0 otherwise

$\beta_i = 1$, if fluid returning from load enters node i, 0 otherwise

$$\gamma_i = \dot{m}_{heat} \sum_{j=1}^{i-1} \alpha_j - \dot{m}_{load} \sum_{j=i+1}^{N} \beta_j$$

$$\delta_i = \begin{cases} 1, & \text{if } \gamma_i > 0 \\ 0, & \text{if } \gamma_i \le 0 \end{cases}$$

$\epsilon = 1$, if auxiliary is on, 0 otherwise.

Equation (2) represents a set of N first-order ordinary differential equations that can be solved analytically for the temperatures of the N nodes as a function of time.

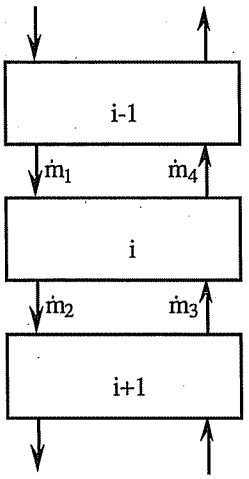

Fig. 1. Internal flows associated with Node i.

2.2 *Plug flow model*

The plug flow model simulates the behavior of a temperature-stratified storage tank using a variable number of variable size segments [1,2,7]. The number of segments and their volumes cannot be controlled but vary, depending primarily on the tank volume, the net (heat source plus load) flow, and the simulation time step. The maximum number of segments in the current TRNSYS implementation is 50. This upper bound is maintained by merging small segments, if necessary. Figure 2 illustrates the operation of this tank model.

In this example, the tank is initially divided into four segments, each of volume V_i and temperature T_i. In one time step, the heat source delivers a volume of liquid, V_{heat}, at a temperature T_{heat}. Assuming that $T_{heat} > T_1$, a new segment is added at the top of the tank, and the entire profile is shifted down. At the same time, a segment of fluid with volume V_{load} and temperature T_{mains} returns from the load. If $T_{mains} < T_4$, a segment is added at the bottom of the tank, and the whole profile is shifted upward. These profile shifts occur simultaneously. The net shift of the initial profile is equal to the difference between the total heat source volume and load volume. The segments and/or fraction of segments whose positions fall outside the bounds of the tank are returned to the heat source and load. A mean value for the temperatures is computed if necessary.

The plug flow model provides the option of fixed and variable inlet positions, as in the multinode model. For both options, the incoming fluid mixes with existing segments if its temperature is within 0.5°C; otherwise, a new segment is created. The plug flow model also allows for the addition of auxiliary energy and conduction between segments.

2.3 *Plume entrainment model*

In the late afternoon or during cloudy periods when the availability of solar energy has decreased and the top portion of the tank is still hot as a result of higher energy input earlier in the day, the temperature of the incoming fluid may be cooler than the upper portion of the tank. As a result, a downward-directed buoyancy force will drive the incoming fluid down into the tank. Due to its turbulent motion and viscosity, the hot fluid in the tank will be entrained in the falling plume. Thus, the incoming stream is heated, and it will fall down to the position in the tank where its density, and therefore temperature, matches that of the tank. This phenomenon is known as "plume entrainment," and it will decrease the degree of stratification in the tank.

The mathematical model of plume entrainment, developed by Phillips and Pate [8], is based on energy and mass balances. The storage tank is modeled as having two separate sections: the plume or stream region and the rest of the tank. These regions will be referred to as the stream (S) and the tank (T) regions,

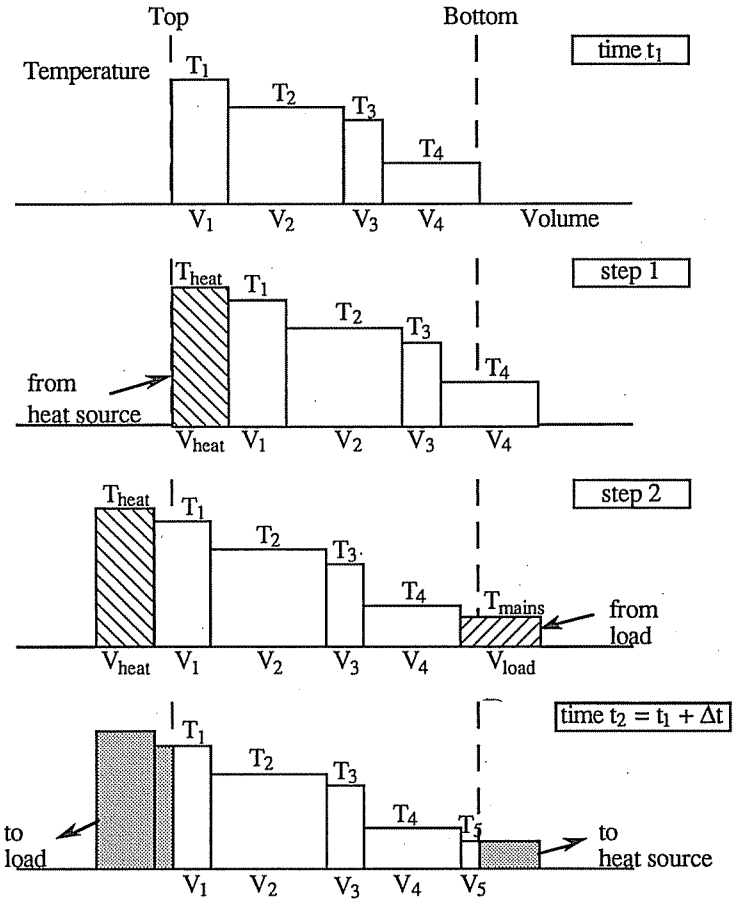

Fig. 2. Concept of the plug flow model.

as shown in Fig. 3. The distance from the top of the tank to where the stream merges with the tank is denoted as d and is defined as the smallest value of x for which the stream temperature exceeds the tank temperature. It is assumed that, except in the vicinity of the stream, there are no horizontal temperature gradients in the tank, which is justified by the experimental work of Pate[10]. A one-dimensional model can therefore be formulated. It is further assumed that the cross-sectional area of the stream is much smaller than that of the tank, so that both axial conduction and the thermal capacity of the stream can be neglected and the tank cross-sectional area can be considered to be constant.

Energy balances are written for the stream

$$C_f \frac{\partial(\dot{m}_S T_S)}{\partial x} = C_f T_T \frac{\partial \dot{m}_S}{\partial x} \tag{3}$$

and for the tank

$$\rho_f A C_f \frac{\partial T_T}{\partial t} = -C_f \frac{\partial(\dot{m}_T T_T)}{\partial x} + C_f T_T \frac{\partial \dot{m}_T}{\partial x} + k_f A \frac{\partial^2 T_T}{\partial x^2} - U_T P_T (T_T - T_{env}). \tag{4}$$

Conservation of mass requires that

$$\frac{\partial \dot{m}_S}{\partial x} = -\frac{\partial \dot{m}_T}{\partial x}. \tag{5}$$

In order to solve for $\dot{m}_S(x, t)$, $\dot{m}_T(x, t)$, $T_S(x, t)$, and $T_T(x, t)$, one additional equation is needed to describe how mass from the tank is entrained into the

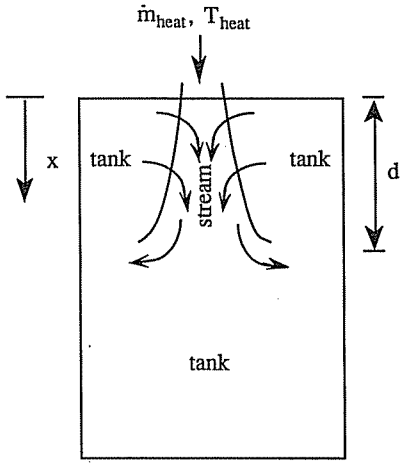

Fig. 3. Stream and tank regions.

falling stream. The mechanistic model for entrainment rates of a plume in a stratified environment can be very complex, as explained by Phillips and Pate[8]. In this study, the mass entrained in the falling stream is assumed to be independent of temperature. The plume is treated as a momentum-driven jet. The theory of isothermal entrainment has been summarized by Schlichting[11]. It has been shown that, for developed axisymmetric flow,

$$\frac{\partial \dot{m}_S}{\partial x} = C\frac{\dot{m}_{heat}}{D}. \tag{6}$$

Numerical values for C under specific conditions can be obtained from the theoretical work summarized by Schlichting and the experimental work of Hill[12]. In this model, C is assumed to be 0.32.

Equations (3–6) were discretized by Lightstone[13]by using a finite volume approach. The tank and stream energy equations were decoupled by delaying the energy lost from the tank into the stream (using tank temperatures from the previous time step), allowing an explicit solution scheme. The solution procedure starts by solving for the stream temperature field, which gives the penetration depth of the stream. After merging the stream with the tank, the tank temperatures can be determined by solving the equations for the tank segments above and below the penetration depth. This plume entrainment model has been incorporated into the TRNSYS multinode and plug flow models.

3. EXPERIMENTAL DATA

3.1 *Low flow system*

The data for the low flow system were taken at Queen's University, Queen's, Kingston, Ontario[14]. The experimental apparatus consisted of a two-component (collector and tank), direct-flow SDHW system, as shown in Fig. 4, and a microcomputer-based data acquisition and control system. The solar collector array was experimentally simulated, using a conventional thermal heat source, as described in ASHRAE standard 95-1981. The collector area was 2.9 m^2, and the values of $F_R(\tau\alpha)$ and $F_R U_L$ were 0.743 and 4.54 W/m^2-K, respectively, at a flow rate of 72 kg/h. The collector loop heater was adjusted every minute to deliver energy equal to that of the specified collector operating under a daily irradiance of 12 MJ/day and the measured heat source return temperature. The daily irradiance profile on the collector surface was simulated as a sinusoidal profile between 0700 and 1700 h of the day. Effects of different flow rates were accounted for by adjusting the collector heat removal factors, F_R, as described in Duffie and Beckman[2]. The collector loop pump was turned on at 0700 h and turned off when the rate of the useful energy gain for the collector dropped below zero in the late afternoon. A storage tank with volume equal to 180 L and length-to-diameter ratio of 1.84 was used. The *UA* value was determined to be 4.57 W/K by raising the tank to a uniform temperature and measuring the rate of temperature decay over time. Water was drawn at a flow rate of 6 L/min from the system. Tests for various collector flow rates and load profiles were performed as shown in Table 1. Successive test days were repeated until the system was determined to be functioning in a "steady-periodic" state. This state was identified when the daily delivered energy was found to vary <3% between test days. The data acquisition and control system supervised load draws, calculated thermal performance (delivered energy), and collected temperature and volume flow rate data every 5 min. Representative experimental tank temperatures plotted in Fig. 5 show very definite stratification.

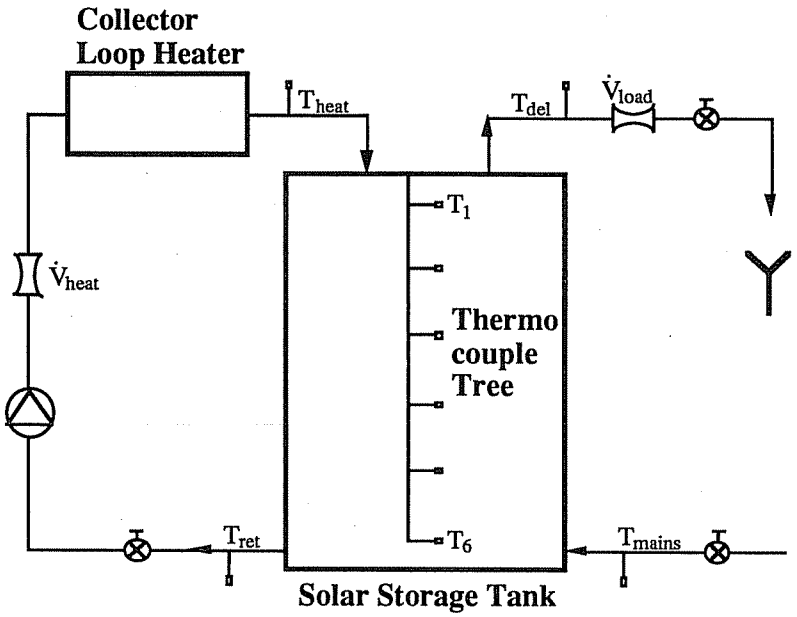

Fig. 4. Experimental setup for the low flow system.

Table 1. Experimental design for the low flow system

Test no.	$\dot{m}_{heat}$ (kg/h)	Load profile	Hour	Profile 1 (L)	Profile 2 (L)	Profile 3 (L)
1	24	Profile 1	7	7	0	10
2	36	Profile 1	8	17	0	25
3	48	Profile 1	9	17	0	25
4	60	Profile 1	10	30	0	45
5	72	Profile 2	11	16	0	25
6	84	Profile 3	12	7	0	10
			13	3	0	5
			14	0	0	0
			15	0	0	0
			16	10	0	15
			17	17	0	25
			18	30	0	45
			19	16	40	25
			20	20	40	30
			21	7	40	10
			22	3	40	5
			23	0	40	0
			Total volume	200	200	300

3.2 *High flow system*

The data for the high flow system were taken at Colorado State University, Fort Collins, Colorado[15], from a drain-back system, as shown in Fig. 6. The experimental test procedure consisted of a test in which the solar radiation and water load profile, ambient temperature (22 ± 2°C), mains water temperature (22 ± 1°C), and hot water set point temperature (≥48.9°C) were specified. The tests were completed at the end of 4 days or when the daily value of the added auxiliary energy was within 3% of the previous day's value, whichever came first. The solar storage tank was preheated to about 40°C at the beginning of the tests to achieve faster convergence. The tests start at 1700 h of the day. Solar radiation input was simulated with an electric boiler downstream of the collector array, located in a constant temperature dark room. The boiler input was controlled according to an hourly profile specified by the Solar Rating and Certification Corporation (SRCC)[16], and calculations were outlined in ASHRAE standard 95-1987. The energy input occured between 0800 and 1700 h of the day. The value of the total radiation was 17.03 MJ/(m^2 − day). The collector parameters, $F_R(\tau\alpha)$ and F_RU_L, were 0.602 and 5.56 W/m^2-K, respectively, at a flow rate of 63.77 kg/h-m^2. Because the collector was not irradiated, a deadband controller for the collector pumps was emulated through the control software.

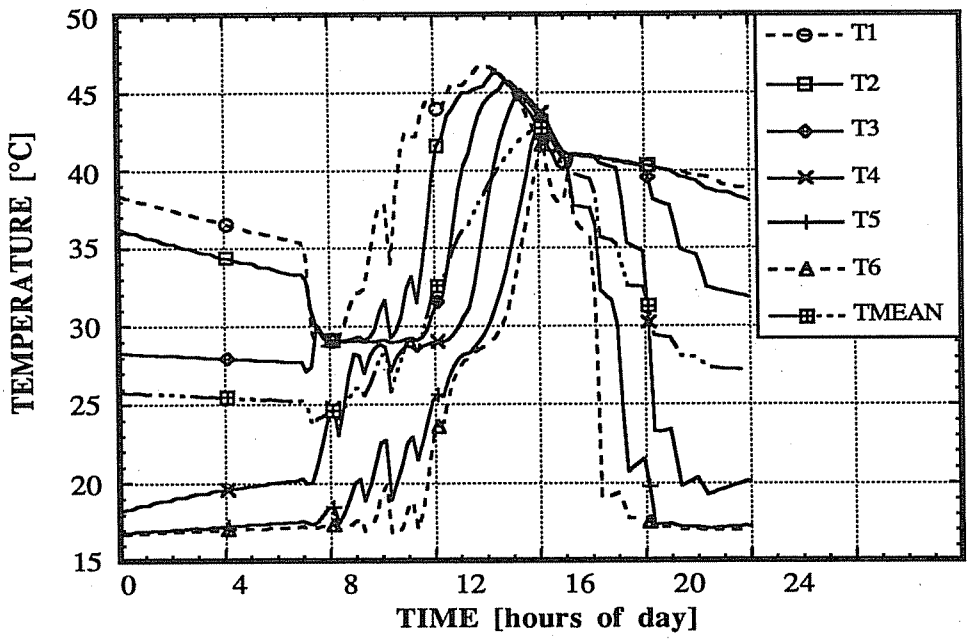

Fig. 5. Tank temperatures for the low flow system.

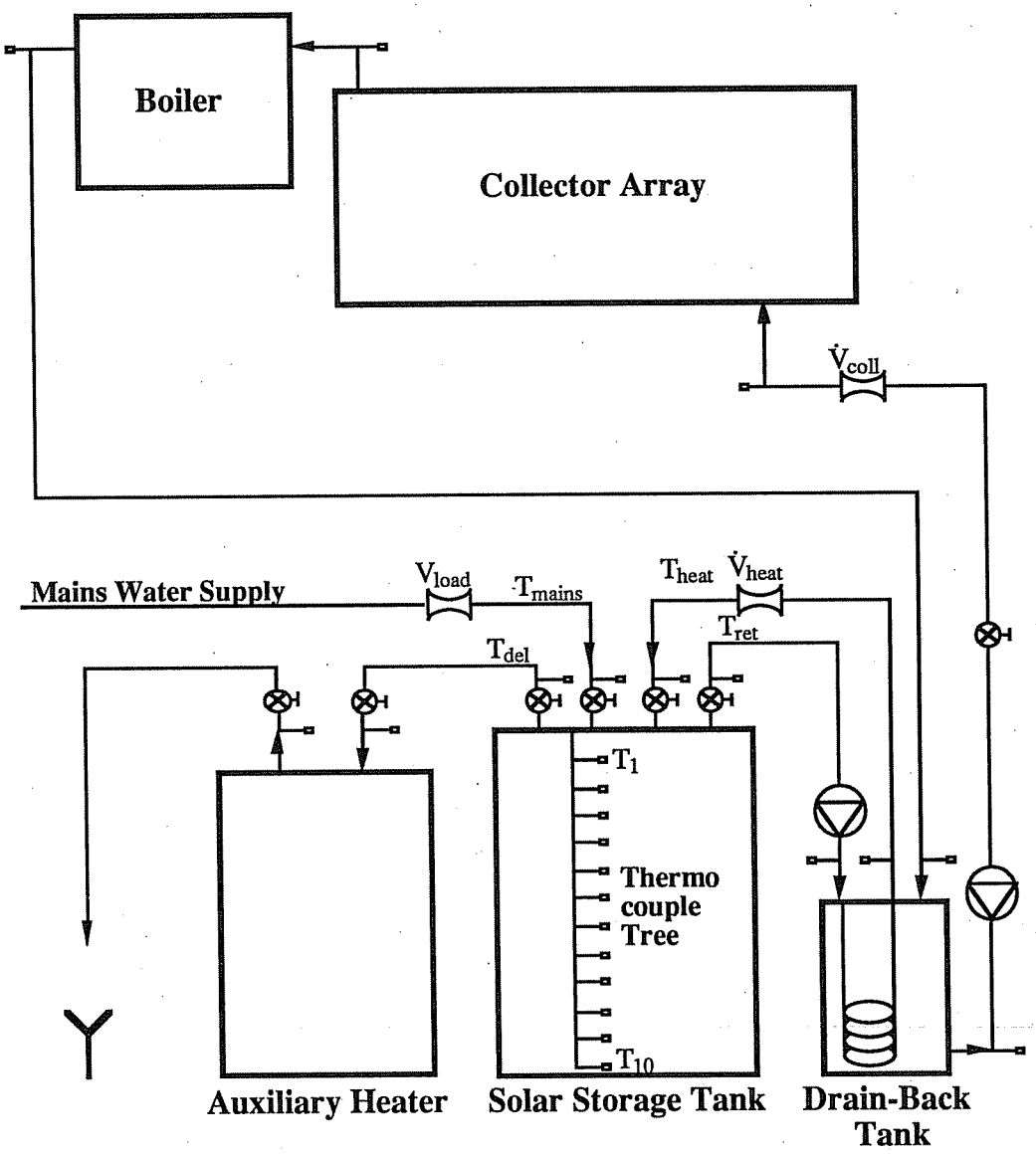

Fig. 6. Experimental setup for the high flow system.

The daily hot water load was based on energy and was made in three equal draws at 0800, 1200, and 1700 h of the day. The energy drawn from the system was specified as 49.8 MJ/day. Each draw required about 130 L of mains water and was performed at a flow rate of 720 kg/h. The *UA* values for the large and small solar storage tank, determined by cool-down tests, were 3.74 and 3.47 W/°C, respectively. The volume of the auxiliary tank was 159 L, and the drain-back tank had a volume of 30 L. Temperatures, volume flow rates, energy usage, and energy delivery were monitored throughout the system. Data were recorded at varying rates during the tests. During a hot water draw, data were recorded every 15 s. Data were recorded every 15 min during simulated daylight hours and every 30 min during overnight periods.

Eight experiments were designed by combining two different storage tank volumes, two values of the collector gross area, and two different heat source flow rates and collector flow rates, as shown in Table 2. Figure 7 shows typical tank temperatures for the solar storage tank, as measured by the thermocouple tree.

Table 2. Experimental design for the high flow system

Test no.	Tank volume (L)	Collector area (m^2)	$\dot{m}_{heat}$ (kg/h)	$\dot{m}_{coll}$ (kg/h)
1	223	2.78	171	205.2
2	223	2.78	342	410.4
3	223	5.56	171	410.4
4	223	5.56	342	205.2
5	272	2.78	171	410.4
6	272	2.78	342	205.2
7	272	5.56	171	205.2
8	272	5.56	342	410.4

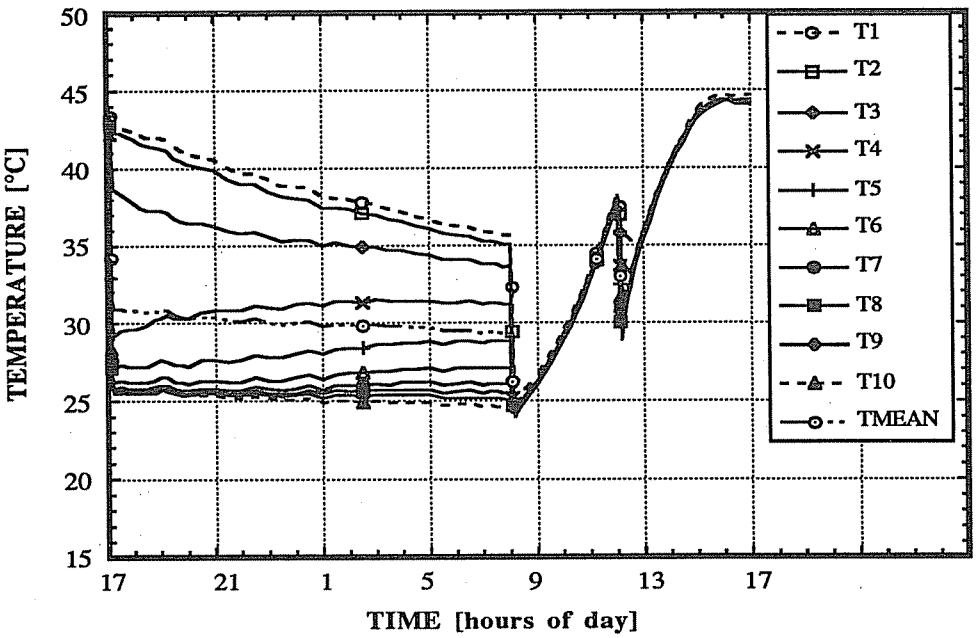

Fig. 7. Tank temperatures for the high flow system.

4. SIMULATION OF THE EXPERIMENTAL DATA

4.1 *System*

The experimental setup for the low flow system was first simulated with a system similar to that shown in Fig. 4 by specifying the energy to the collector, the flow rates, and the mains water temperature. With this method of simulating the experimental data, the equations describing the performance of the collector and tank were found to be highly coupled. If, for example, the tank model predicted an incorrect temperature returned to the collector, then the collector added an incorrect value of useful energy, resulting in an incorrect collector output temperature. This incorrect temperature was used as tank input temperature, which then affected the temperature of the fluid delivered to the load and the temperature of the fluid returned to the collector. The coupled system caused incorrect inputs to the tank, confounding the comparison with experimental data.

It is necessary to have correct inputs in order to validate a system component model. In this study, the input values of temperature and flow rate for the tank were forced to be the same as those measured in the experiments. Forcing the inputs to be the experimental values in TRNSYS required the use of time-dependent forcing functions and small time steps.

4.2 *Performance numbers*

Comparisons were initially made between the experimental and simulated top and bottom tank temperatures. However, no pattern could be recognized in these comparisons. In addition, a complication arose in that the top and bottom temperatures represented by the models were at different locations for the multinode model, depending on the number of nodes, and at variable locations for the plug flow model due to the adaptive size of the segments. This complication could be avoided by comparing the experimental and simulated mean tank temperatures. There was again no recognizable pattern that allowed any judgment on the performance of the different tank models.

Three numbers have been defined in order to compare the simulated outputs with experimental outputs. For the load side (discharging), QD is defined as the difference between the predicted and the measured delivered energy divided by the experimentally delivered energy:

$$QD = \frac{Q_{\text{del,sim}} - Q_{\text{del,exp}}}{Q_{\text{del,exp}}}$$

$$\text{with} \quad Q_{\text{del}} = \int_{\text{day}} \dot{m}_{\text{load}} C_{\text{f}} (T_{\text{del}} - T_{\text{mains}}) dt. \quad (7)$$

QD is a measure of the ability of the model to predict the temperature of the fluid delivered to the load. For the heat source side (charging), QI is defined as the difference between the simulated and the experimental energy input from the heat source divided by the measured energy input:

$$QI = \frac{Q_{\text{in,sim}} - Q_{\text{in,exp}}}{Q_{\text{in,exp}}} \quad \text{with}$$

$$Q_{\text{in}} = \int_{\text{day}} \dot{m}_{\text{heat}} C_{\text{f}} (T_{\text{heat}} - T_{\text{ret}}) dt. \quad (8)$$

QI is a measure of the ability of the model to predict the temperature of the fluid returned to the heat source. A second number has been defined for the heat source side, which is also a measure of the ability of the model to predict the heat source return temperature, but does

not allow the compensation of deviations of $T_{ret,sim}$ from $T_{ret,exp}$ to both sides. This dimensionless performance number P is

$$P = \frac{\sqrt{\sum_{t=t_{on}}^{t_{off}} \dot{m}_{heat}^2 C_f^2 (T_{ret,exp} - T_{ret,sim})^2 \Delta t^2}}{\int_{day} \dot{m}_{heat} C_f (T_{heat} - T_{ret,exp}) dt}. \quad (9)$$

The denominator represents the experimental energy input into the tank. The numerator is a sum of the squared errors in the energy input into the tank. The values of P are determined by both the magnitude of the heat source flow rate and the magnitude of the temperature errors $T_{ret,exp} - T_{ret,sim}$.

5. RESULTS

5.1 *Performance numbers*

Figures 8 and 9 show results for *QI*, *QD*, and *P* obtained for test 2 of the low flow system. The fully mixed tank model significantly underpredicts the experimentally measured energy quantities. For the other models, differences due to fixed inlets, variable inlets, or included plume entrainment can be noted. The plug flow models with fixed and variable inlets tend to overpredict the energy quantities. Including plume entrainment in the plug flow model works well under the considered conditions. A large number of nodes is necessary for the multinode models to represent the experimental data. These results also indicate the limitations of the fully mixed tank model. The use of the multinode models with a large number of nodes shows the best agreement with the experiment. The *P* index suggests that the plug flow model is about as good as a three-node tank model.

Figures 10 and 11 show results for *QI*, *QD*, and *P* for test 4 of the high flow system. The fully mixed tank model leads to an underprediction in the experimentally measured energy quantities, but less underprediction than that for the low flow case. The plug flow models overpredict the energy quantities. Two or three nodes work well for the multinode models with fixed or variable inlets. Four nodes give the best result for the multinode model with plume entrainment. An increase in the number of nodes results in an overprediction of the energy quantities for the multinode models.

5.2 *Choice of number of nodes*

Because the performance of the multinode models depends on the chosen number of nodes, a relationship between the number of nodes and the conditions under which the tank operates is needed. The quantities that were varied significantly during the experiments or simulations are the values of the heat source flow rate, the load draw profiles (only for the low flow system), the collector area, and the collector flow rate (the latter two quantities for the high flow system only). The variation of the collector area and the collector flow rate have little influence on the results obtained for a multinode model with a particular number of nodes. Therefore, relations between the number of nodes and mean number of tank turnovers, T, for fixed and variable inlets were developed. Equations (10) and (11) relate the recommended number of nodes to the tank turnovers for fixed and variable inlets, respectively:

$$N_{fixed} = 45.8 T^{-1.218} \quad (10)$$

$$N_{variable} = 23.1 T^{-0.966}. \quad (11)$$

The recommended number of nodes is the smallest possible number of nodes for which the relative errors in the energy quantities *QI* and *QD* do not exceed 5% and the performance number P is within 10% of the best value of P, P_{best}. These criteria were established

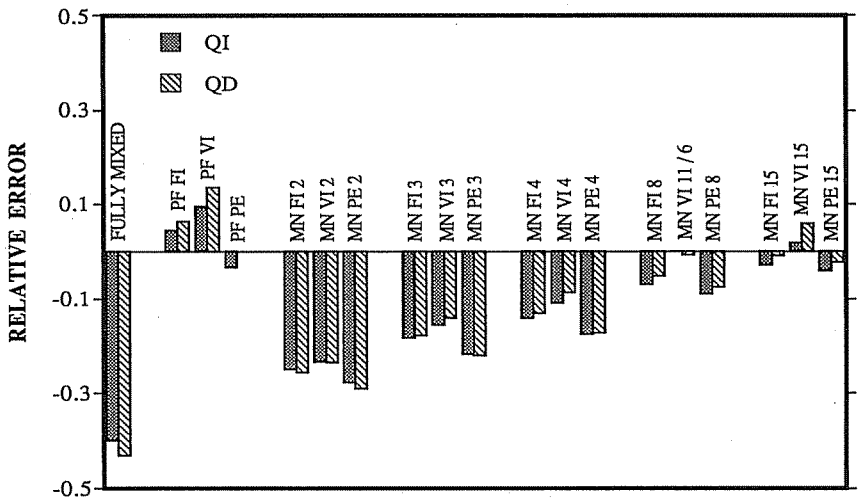

Fig. 8. Results for *QI* and *QD* for low flow test 2. (PF = plug flow; MN = multi-node; PE = plume entrainment; FI = fixed inlets; VI = variable inlets; N = # of nodes.)

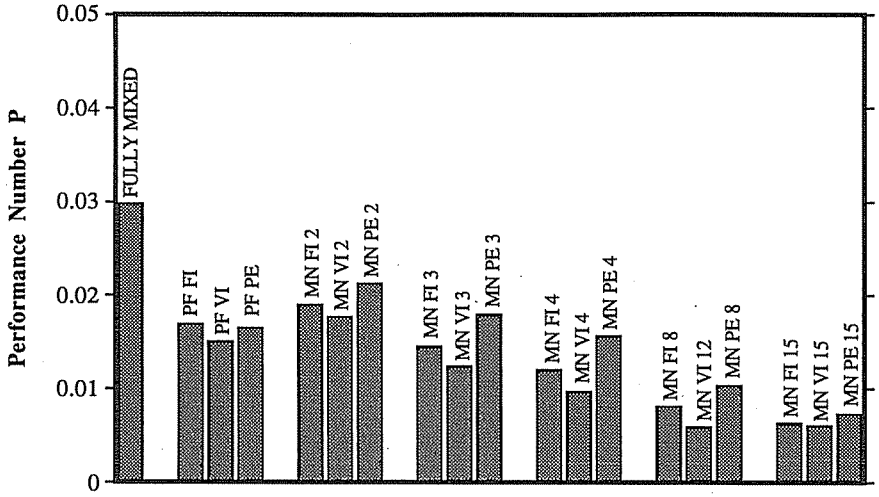

Fig. 9. Results for P (eqn [9]) for low flow test 2. (PF = plug flow; MN = multinode; PE = plume entrainment; FI = fixed inlets; VI = variable inlets; N = # of nodes.)

with two considerations. First, the number of nodes that gives the best results for QI, QD, and P was often found to be 15 for low flow rates, indicating that the performance numbers might be improved if the number of nodes could have been further increased. From this point of view, 15 nodes is an artificially introduced maximum number of nodes. By introducing the above 5 and 10% criteria, it was possible in 11 out of 17 cases to avoid the artificial limit of 15 nodes. The errors in predicting the energy quantities, when using the number of nodes proposed by the fitted curves, showed not more than 13% deviation from the experimental results[17].

5.3 *Time-step dependence*

The performance of both the plug flow and the multinode models depends on the simulation time step. To investigate this dependence, simulations were performed with a simple system consisting of a collector (2.9 m^2) and a tank (180 L). Hourly radiation and load profiles were specified and time steps ranging from 1 to 60 min were used. The values of the delivered energy were taken as the criteria for the time-step dependence. The results for two different collector flow rates of 20 and 180 kg/h are shown in Figs. 12 and 13.

For the collector flow rate of 20 kg/h, all the models, except the plug flow model with plume entrainment, exhibit a change in delivered energy with respect to the value for the time step of 60 min of <1.5%. The value of delivered energy for the plug flow model with plume entrainment changes by 8%. For the collector flow rate of 180 kg/h, all the models, except the plug flow model with variable inlet, show a change of <3.3%. For the plug flow model with variable inlet, the relative change in delivered energy is 9%. In both cases a plug

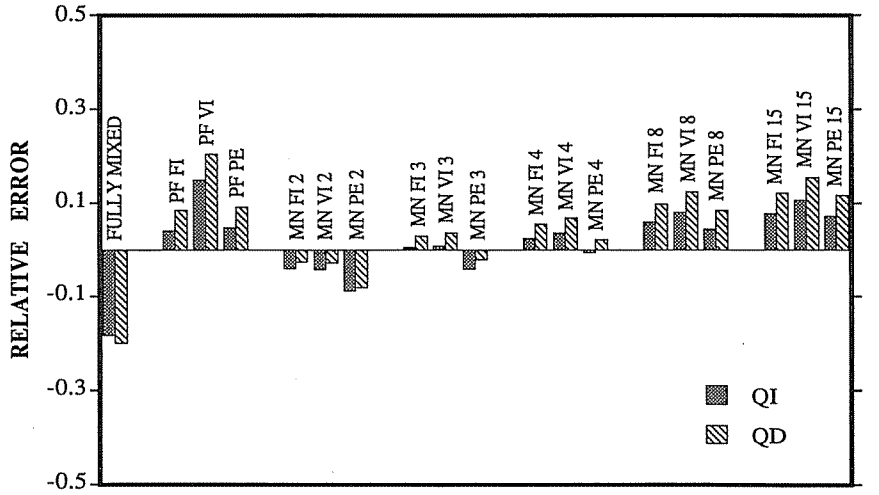

Fig. 10. Results for QI and QD for high flow test 4. (PF = plug flow; MN = multi-node; PE = plume entrainment; FI = fixed inlets; VI = variable inlets; N = # of nodes.)

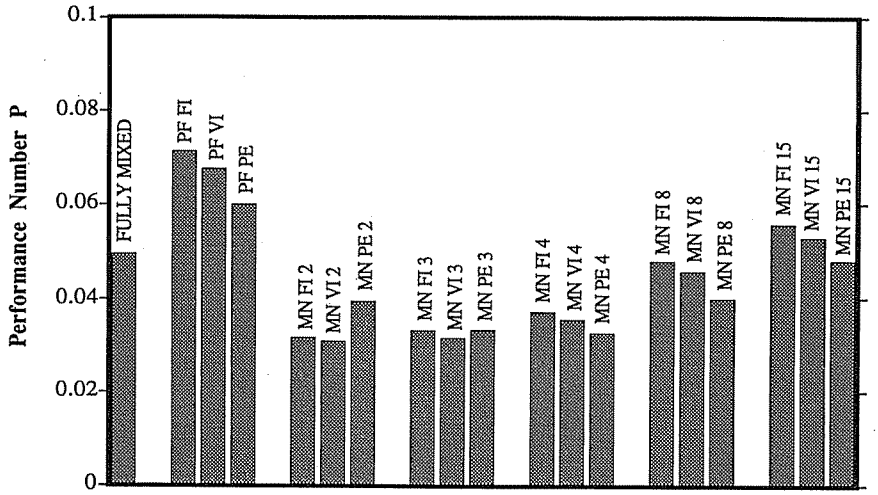

Fig. 11. Results for P (eqn[9]) for high flow test 4. (PF = plug flow; MN = multi-node; PE = plume entrainment; FI = fixed inlets; VI = variable inlets; N = # of nodes.)

flow model shows the greatest difference. This difference is related to the change in the daily average number of segments employed as a function of the simulation time step. The two models that exhibit the greatest change in the average number of segments also have the poorest time-step dependence.

5.4 *Computational efficiency*

The selected models also were compared with respect to their computational efficiency. A simple TRNSYS deck with three forcing functions, one integrator, one printer, and the tank model under investigation was set up to simulate 200 similar days for various heat source flow rates and time steps. The heat source flow rate operated 8 h/d. The temperature of the fluid from the heat source was specified as an hourly step profile with first rising and then falling temperatures in order to force the variable inlet option and plume entrainment to be employed. An hourly load profile was specified with four equal draws equally distributed during the time of the heat source flow. The simulations were performed on a VAX station 3100 model 38. Table 3 shows the CPU seconds for the different tank models, obtained by subtracting the CPU time for simulating the deck without tank model from the CPU time for simulating the deck including the tank model.

The plug flow models are faster for the higher heat

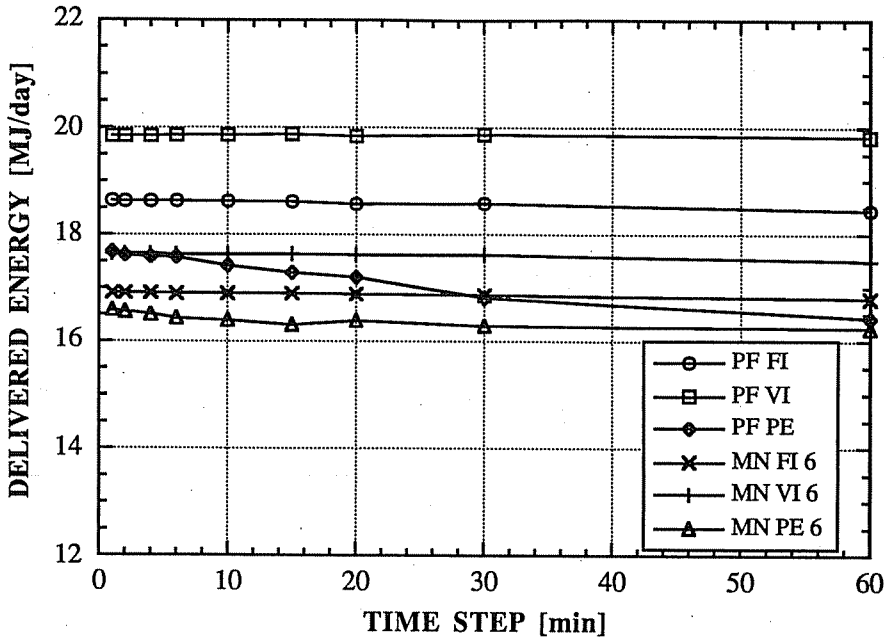

Fig. 12. Time step dependence of the tank models for a collector flow rate of 20 kg/h. (PF = plug flow; MN = multi-node; PE = plume entrainment; FI = fixed inlets; VI = variable inlets.)

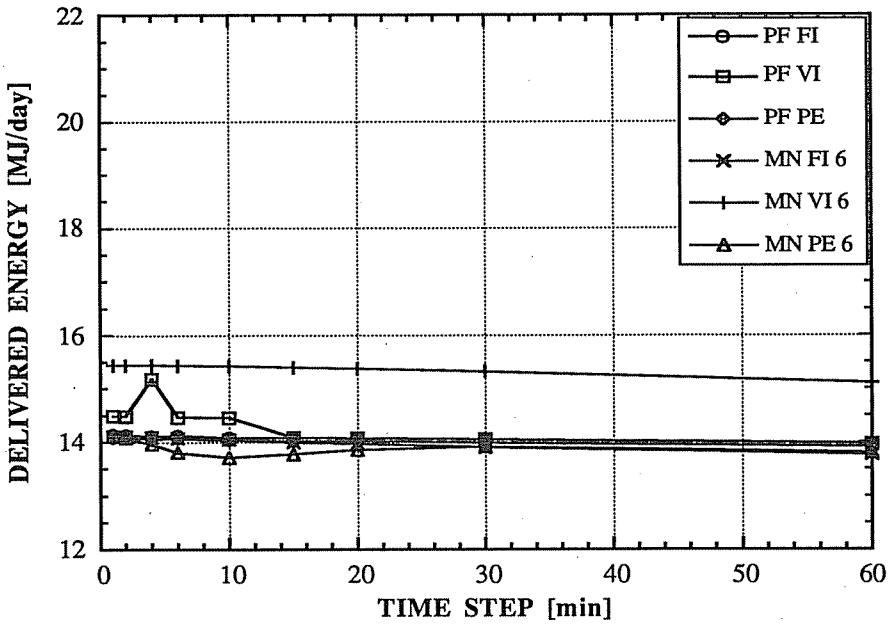

Fig. 13. Time step dependence of the tank models for a collector flow rate of 180 kg/h. (PF = plug flow; MN = multi-node; PE = plume entrainment; FI = fixed inlets; VI = variable inlets.)

source flow rate (200 kg/h) than for the lower heat source flow rate (25 kg/h), because the higher heat source flow rate results in a smaller number of nodes. The CPU times for the multinode models depend strongly on the specified number of nodes. The plug flow models are faster than the multinode models. For the lower heat source flow rate, the plug flow model with variable inlets uses significantly more CPU time than the other plug flow models due to a large number of segments involved in the algorithms for finding the heat source flow inlet position. Including plume entrainment significantly increases the CPU time for the large simulation time step and the high heat source flow rate for the multinode models.

Table 3. CPU seconds for the different tank models on a VAX station 3100 model 38

	Heat source flow rate			
	(25 kg/h) Simulation time step		(200 kg/h) Simulation time step	
Tank model	1 h	0.1 h	1 h	0.1 h
PF FI	3.01 s	40.72 s	2.21 s	25.81 s
PF VI	5.05 s	71.5 s	2.32 s	26.53 s
PF PE	2.95 s	42.06 s	3.48 s	28.48 s
Fully mixed	3.7 s	37.77 s	3.56 s	38.83 s
MN FI 3 nodes	6.37 s	64.53 s	6.35 s	63.77 s
MN VI 3 nodes	6.45 s	64.18 s	6.05 s	66.63 s
MN PE 3 nodes	7.05 s	71.48 s	14.09 s	71.03 s
MN FI 15 nodes	17.2 s	177.27 s	17.5 s	181.23 s
MN VI 15 nodes	19.16 s	179.97 s	18.15 s	180.07 s
MN PE 15 nodes	21.47 s	174.74 s	51.57 s	191.81 s

PF = plug flow model; MN = multinode model; PE = plume entrainment; FI = fixed inlets; VI = variable inlet.

The small increase in CPU time for the plug flow model including plume entrainment for a high heat source flow rate and a large simulation time step is due to the fact that the employed number of segments is very low (mostly one).

6. CONCLUSIONS

Several one-dimensional models for stratified thermal storage tanks have been investigated and compared to experimental data for a wide range of conditions. The goal of this study was to give some recommendations as to which tank model should be used under which conditions in energy systems simulations. The assumption of a uniform tank temperature (instantaneous mixing) leads to a considerable underprediction of the energy input into the tank and the delivered energy under all considered conditions. The relationships between the recommended number of nodes and the mean number of tank turnovers are useful as a guideline for choosing the most appropriate number of nodes under given operating conditions. Use of the multinode model with variable inlets is recommended, as this model requires fewer nodes than the multinode model with fixed inlets for equivalent accuracy and is therefore computationally more efficient. The plug flow models are computationally more efficient than the multinode models, but both the fixed and the variable inlet models tend to overpredict energy quantities. Use of the plug flow model including plume entrainment is recommended as an alternative to the multinode with variable inlets for a mean number of tank turnovers lower than five. Care should be taken in choosing the simulation time step because results obtained with the plug flow models were found to depend on the simulation time step.

Acknowledgments—The authors wish to thank Professor S. J. Harrison of Queen's University, Kingston, Ontario, and Professor J. Davidson of Colorado State University, Fort Collins, Colorado, for providing the experimental data that made this study possible.

NOMENCLATURE

A (m^2)	cross-sectional area of the tank
C (-)	(entrainment) constant
C_f (kJ(kg-K))	specific heat capacity of the fluid
D (m)	inlet pipe diameter
F_R (-)	collector heat removal factor
k_f (kJ/h-m-K)	thermal conductivity of the fluid
$\dot{m}$ (kg/h)	mass flow rate
$\dot{m}_{heat}$ (kg/h)	mass flow rate in the heat source loop
$\dot{m}_{load}$ (kg/h)	mass flow rate in the load loop
$\dot{m}_S$ (kg/h)	mass flow rate of the stream
$\dot{m}_T$ (kg/h)	mass flow rate of the tank
M_{heat} (kg)	total daily mass of the heat source fluid
M_i (kg)	mass of the fluid in the ith node
M_{load} (kg)	total daily mass of the load fluid
M_T (kg)	mass of the fluid in the tank
N (-)	number of nodes
P (-)	performance number
P_{best} (-)	best value of P (for a particular test)
P_T (m)	perimeter of the tank
$\dot{Q}_{aux,i}$ (kJ/h)	rate of auxiliary energy input into node i
QD (-)	relative error in the delivered energy
Q_{del} (kJ)	delivered energy
QI (-)	relative error in the energy input into the tank
Q_{in} (kJ)	energy input into the tank
t (h)	time
Δt (h)	time step
t_{off} (h)	time when flow from heat source ends
t_{on} (h)	time when flow from heat source begins
T (-)	mean number of tank turnovers
T_{del} (°C)	temperature of the fluid delivered to the load
T_{env} (°C)	temperature of the environment
T_{fl} (°C)	average flue temperature
T_{heat} (°C)	temperature of fluid from the heat source
T_i (°C)	temperature of the ith node
T_{mains} (°C)	mains water temperature
T_{mean} (°C)	mean tank temperature
T_{ret} (°C)	temperature of fluid returned to heat source
T_S (°C)	temperature of the stream
T_T (°C)	temperature of the tank
U_L (kJ/(m^2 h °C))	heat loss coefficient of collector per unit area
U_T (kJ/(m^2 h °C))	heat loss coefficient of tank per unit area
UA (kJ/(h °C)	heat loss coefficient of the tank
$UA_{fl,i}$ (kJ/(h °C))	heat loss coefficient to the gas flue of an in-tank auxiliary heater for node i
$\dot{V}_{coll}$ (m^3/s)	volume flow rate in the collector loop
V_{heat} (m^3)	volume of fluid from the heat source
$\dot{V}_{heat}$ (m^3/s)	volume flow rate in the heat source loop
V_i (m^3)	volume of node i
V_{load} (m^3)	volume of fluid returned from the load
$\dot{V}_{load}$ (m^3/s)	volume flow rate in the load loop
x (m)	vertical distance from the top of tank
ρ_f (kg/m^3)	density of the fluid
$(\tau\alpha)$ (-)	transmittance–absorptance product
exp	experimental
sim	simulated

REFERENCES

1. S. A. Klein et al., *TRNSYS* 13.1 User's manual, Engineering Experiment Station Report 38-13, Solar Energy Laboratory, University of Wisconsin–Madison (1990).
2. J. A. Duffie and W. A. Beckman, *Solar engineering of thermal processes,* 2nd ed., Wiley Interscience, New York (1991).
3. M. D. Wuestling, S. A. Klein, and J. A. Duffie, Promising control alternatives for solar water heating systems, *ASME. J. Solar Energy Eng.* **107,** 215–221 (1985).
4. M. K. Sharp and R. I. Loehrke, Stratified thermal storage in residential solar energy applications, *J. Energy,* **3**(2), 106–113 (1979).
5. W. F. Phillips and R. N. Dave, Effects of stratification on the performance of liquid-based solar heating systems, *Solar Energy,* **29,** 111–120 (1982).
6. S. A. Klein, A design procedure for solar heating systems, Ph.D. Thesis, Department of Chemical Engineering, University of Wisconsin–Madison (1976).
7. J. K. Kuhn, G. F. VanFuchs, and A. P. Zob, Developing and upgrading of solar system thermal energy storage simulation models, Draft Report for DOE, Boeing Computer Services Company (August 31 1980).
8. W. F. Phillips and R. A. Pate, Mass and energy transfer in a hot liquid energy storage system, *Proceedings of the American Section of the International Solar Energy Society,* Orlando, FA (1977).
9. Y. H. Zurigat, K. J. Maloney, and A. J. Ghajar, A comparison study of one-dimensional models for stratified thermal storage tanks, *Trans. ASME,* **111,** 204–210 (1989).
10. R. A. Pate, A thermal energy storage tank model for solar heating, Ph.D. Thesis, Utah State University, Logan, UT (1977).
11. H. Schlichting, *Boundary layer theory,* 6th ed., McGraw-Hill, New York (1968).
12. B. J. Hill, Measurements of local entrainment rate in the initial region of axisymmetric turbulent air jet, *J. Fluid Mech.,* **51,** 773–779 (1972).
13. M. Lightstone, *Mathematical model of plume entrainment,* Solar Thermal Research Laboratory, University of Waterloo, Ontario, (1987).
14. R. J. Cataford and S. J. Harrison, Factors affecting storage tank stratification and the thermal performance of SDHW systems, SESCI '90, Hallifax, Nova Scotia, (1990).
15. W. T. Carlson, Comparison of experimental and TRNSYS SRCC ratings of a generic drain-back solar water system, M.S. Thesis, Colorado State University, Fort Collins, CO (1990).
16. Solar Rating and Certification Corporation, Test methods and minimum standards for certifying solar water heating systems, Standard 200–82, Washington, DC (1984).
17. E. M. Kleinbach, Performance study of one-dimensional models for stratified thermal storage tanks, M.S. Thesis, Department of Chemical Engineering, Solar Energy Laboratory, University of Wisconsin–Madison, WI (1990).